JOURNAL INDIAN ASSOCIATION OF SEDIMENTOLOGISTS ISSN NO 2582 – 2020
Vol. 41, Issue I, 2024, pp. 55 – 67
DOI: https://doi.org/10.51710/jias.v41iI.355

Provenance of sediments and environmental risk assessment of heavy metals in the "Mis Amores" beach, Veracruz, Gulf of Mexico, Mexico

Mayla A. Ramos-Vázquez[1,*], John S. Armstrong-Altrin[2,3], Gloria D. Fernández-Guevara[4], Jayagopal Madhavaraju[5], Sanjeet K. Verma[1], and Rathinam Arthur James[3]

[1] División de Geociencias Aplicadas, Instituto Potosino de Investigación Científica y Tecnológica (IPICYT), Camino a la Presa San José 2055, San Luis Potosí 78216, México
[2] Universidad Nacional Autónoma de México, Instituto de Ciencias del Mar y Limnología, Unidad de Procesos Oceánicos y Costeros, Ciudad Universitaria, Ciudad de México 04510, Mexico
[3] Department of Marine Sciences, Bharathidasan University, Tiruchirappalli, 620024, Tamil Nadu, India
[4] Posgrado en Ciencias del Mar y Limnología, Universidad Nacional Autónoma de México, Ciudad Universitaria, 04510 Mexico City, CDMX, Mexico.
[5] Estación Regional del Noroeste, Instituto de Geología, Universidad Nacional Autónoma de México,
E-mail address: mayla.ramos@ipicyt.edu.mx

ABSTRACT

In this study, grain-size, mineralogy, and geochemistry of Mis Amores (MA) beach sediments, Tuxpan, Veracruz State, Gulf of Mexico are analyzed. The textural parameters reveal that the sediments are fine-grained and vary from well-sorted to very well-sorted nature. The SEM-EDS analysis reveal that the sediments are abundant in minerals such as quartz, alkali feldspars, zircon, ilmenite, and pyroxene. Geochemically, the sediments are classified as sub-arkose type. The Chondrite normalized rare earth elements (REE) pattern suggest that the source area is dominated by felsic and intermediate igneous rocks (Eu/Eu^{*} = 0.90 - 1.19, number of samples n = 16). The provenance discrimination diagrams indicated that the MA sediments were derived by the weathering of felsic igneous rocks, probably from the Trans Mexican Volcanic Belt. The results of this study reveal that the Tuxpan River played an important role in delivering sediments to the MA beach area.

The environmental indices suggest that the sediments are moderately contaminated by Zn and moderate to extremely contaminated by Cu and As. The Cu (> 84%) and Zn (> 82%) concentrations are predominantly associated with the exchangeable fraction, which are readily bioavailable. Cu, As, and Zn in the MA sediments were derived from the agricultural activities and waste water discharges from the sanitary network of the Tuxpan town and port.

Keywords: Environmental pollution, provenance, clastic sediments, heavy metals, tectonic setting

INTRODUCTION

Coastal or transitional environment constitutes the limit between continental and marine environments, which are active due to tides, rivers, wave and wind actions (Martínez et al., 2007; Davis and Fitzgerald, 2020). Many studies during the last decade have focused on the characterization of coastal sediments (Bela et al., 2023; Ramos-Vázquez et al., 2022). These studies discussed the provenance changes due to coastal processes (erosion and accretion), precipitation, river and coastal runoff, compositional variations and, biological and anthropogenic factors due to industrial and agricultural activities.

The detrital sediments are the products of weathering, erosion, and transport. Geochemical properties of clastic sediments may be modified during alteration and metamorphism; however, the immobile trace and REE concentrations can be utilized to infer provenance (Tawfik et al., 2018; Nikunj et al., 2023; Paul et al., 2023). The mineralogical components and heavy mineral assemblages in sediments are useful to determine their provenance (Resmi and Achyuthan, 2018; Jiang et al., 2022). The chemical behavior of REE and their resistance to chemical mobilization in sediments have been used as provenance indicators (Ramos-Vázquez et al., 2018). In addition, provenance of sediments can be inferred through textural, mineralogical, chemical, and geochronological variations (Wang et al., 2018). There are studies focused on the mineralogical and geochemical characteristics of beach sediments along the Gulf of Mexico (Campeche to Tamaulipas) (Tapia-Fernández et al., 2017; Armstrong-Altrin et al., 2018, 2021; Armstrong-Altrin, 2020; Ramos-Vázquez and Armstrong-Altrin, 2019, 2021). These studies also interpreted the possible contamination by heavy metals as well as the sediment provenance.

The trace metals originated due to natural (erosion and weathering) and anthropogenic (industrial and mining activities) sources can easily transfer into the marine environment, via municipal and industrial discharges (Nagarajan et al., 2019; Gülşen-Rothmund et al., 2023). Several chemical indices were utilized in various studies to calculate the enrichment of heavy metals in sediments and to differentiate the natural and anthropogenic origin of metals in sediment (Yang et al., 2021; Cai et al., 2023).

In this study, we analyzed the texture, mineralogy, and geochemical composition of sediments collected in the Mis Amores (MA) beach near Tuxpan, Veracruz State, Gulf of Mexico. The objective of this study is to infer the provenance characteristics of sediments. In addition, we utilized the chemical indices such as Enrichment Factor (EF; Zoller et al., 1974), Geoaccumulation Index (I_{geo}; Müller, 1969), Adverse Effect Index (AEI; Long et al., 1995), and Pollution Load Index (PLI; Tomlinson et al., 1980) to identify the possible source of contaminants.

Study Area

Gulf of Mexico is a region with enormous maritime and oil exploration activities. In the southern region of the Veracruz State, pollution has increased due to the operation of petrochemical industries in the Coatzacoalcos region (Aquino-Gaspar et al., 2021). MA beach is located near the mouth of the Tuxpan River, Veracruz State, western Gulf of Mexico (Fig. 1). The Tuxpan River Basin is located in the eastern portion of Mexico, covering an area of 5837 km^2 of the Veracruz (72.1%), Puebla (15.2%), and Hidalgo (12.7%) States (INEGI,2016). The tributary rivers are Pantepec, Vinazco, Buenavista, Tuxpan, and Tecomate stream (INECC, 2018).

Winds in the Gulf of Mexico have important seasonal influences. During winter, the Gulf is influenced by cold air masses coming from the north, which cause strong cold fronts (Zavala et al., 2014). During summer, the currents in the Tamaulipas and Veracruz states flow north, while in the fall and winter seasons the current flows south until it reaches the Bay of Campeche, where it meets an opposing current that runs along the coast (Zavala et al., 2003).

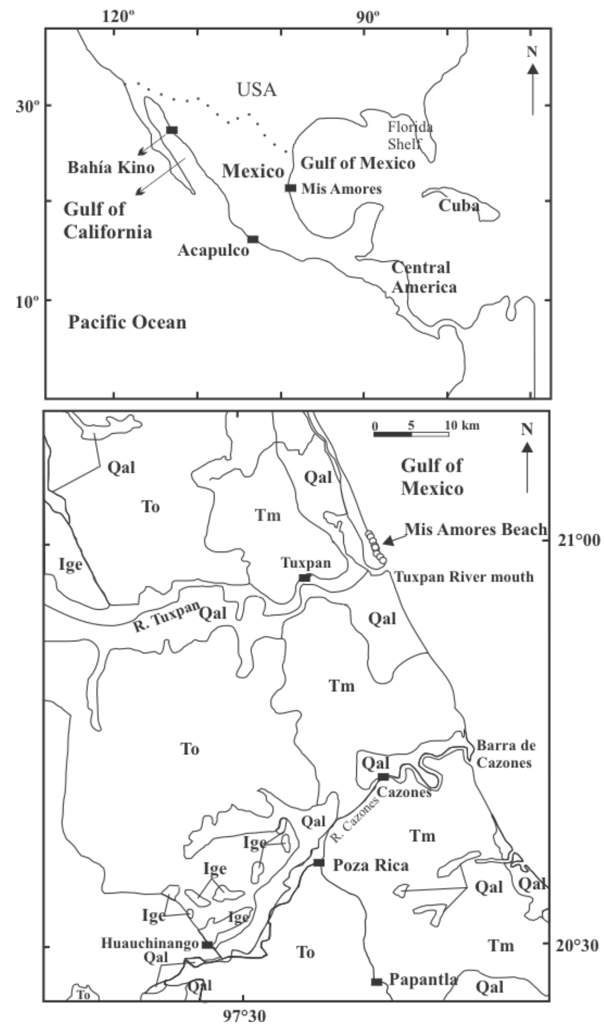

Fig. 1 Map showing sample locations in the Mis Amores beach, Veracruz State, Gulf of Mexico. Map modified after Armstrong-Altrin (2009). Volcanic and sedimentary units are: Ig = intrusive igneous rocks; Ige = extrusive igneous rocks (andesite); Jss = sedimentary rocks (lower Jurassic); Mi = intrusive rocks (Mesozoic); Pz = metamorphic rocks (Proterozoic); Qal = alluvium (Quaternary); Tiv = volcanic rocks (lower Tertiary); Tivc = volcanoclastic rocks (lower Tertiary); Tm = marine rocks (Tertiary; sandstone, mudstone); To = sandstone and limestone (Oligocene); Tsc = clastic rocks (upper Tertiary).

METHODOLOGY

Totally, 16 sediment samples, approximately 2 kg were collected in the swash zone of the "Mis Amores" beach. Granulometric analysis was carried out by the Ro-Tap Sieve Shaker located at Institute of Marine Sciences and Limnology (ICML), Mexico City. All 20 samples were air-dried and sieved through ASTM sieves for 20 minutes (No. 12, 14, 16, 20, 35, 60, 80, 100, 12, 140, 170, 200, and 230 µm).

SEM-EDS

Five selected samples were analyzed by a JEOL JXA-8900R electron microprobe, which is housed in the Institute of Geophysics, UNAM, Mexico City. Peak counting times were 40 s for each element, except for Na and K with counting time 10s.

GEOCHEMISTRY

Sixteen sediment samples were powdered by an agate mortar (< 75 µm) and their major element concentrations were determined using a Thermo Scientific Niton FXL 950 X-ray Fluorescence (XRF). Accuracy of major element analysis was monitored by an international standard JGB1 (GSJ). Loss on ignition was obtained by weighing after combustion 1 h at 1000° C. Concentrations of trace and rare earth elements were determined by a digestion method using aqua regia leach at 95 °C, 0.5 g sample was digested in a microprocessor-controlled digestion block, then analyzed by the ICP-MS using a Perkin Elmer Sciex Elan 9000. The operation procedure to measure trace element concentrations was similar as detailed in Jarvis (1988). The United States Geological Survey Standard BCR-2 (Basalt, Columbia River) was used and the analytical precision of trace elements was less than 5%. Eu and Ce anomalies are calculated as $Eu/Eu^* = Eu_{CN}/[(Sm_{CN})(Gd_{CN})]^{1/2}$ and $Ce/Ce^* = Ce_{CN}/[(La_{CN})(Pr_{CN})]^{1/2}$, respectively ($_{CN}$ chondrite normalized values are from Taylor and McLennan 1985).

STATISTICAL ANALYSIS

Pearson's correlation analysis was performed using Microsoft Excel 2010.

RESULTS

GRAIN SIZE ANALYSIS

The sediments are associated predominately with medium to fine-grained sand. The textural parameters like sorting, skewness, and kurtosis, reveal that the sediments are moderately sorted, near symmetrical, and leptokurtic, respectively (Table 1).

Table 1 Grain size and textural parameters for the Mis Amores beach sediments, Gulf of Mexico (Folk and Ward 1957)

Sample	Mz (θ)	Sorting (θ)	Skewness	Kurtosis
MA1	2.76	0.29	-0.08	1.19
MA3	2.74	0.33	-0.30	1.18
MA5	2.78	0.40	-1.26	1.06
MA7	2.75	0.32	-0.23	1.23
MA9	2.72	0.33	-0.15	0.94
MA11	2.69	0.40	-0.24	1.09
MA13	2.76	0.30	-0.13	1.03
MA15	2.73	0.37	-0.23	1.31
MA17	2.85	0.23	-0.01	0.91
MA19	2.82	0.25	-0.08	0.93
MA21	2.86	0.25	-0.04	1.05
MA23	2.83	0.24	-0.1	1.00
MA25	2.88	0.26	-0.1	1.04
MA27	2.88	0.23	-0.04	0.98
MA29	2.80	0.25	-0.07	1.02
MA31	2.88	0.24	-0.05	1.36
Mean	2.80	0.29	-0.19	1.08
SD	0.06	0.06	0.30	0.13

SEM-EDS

The mineral composition in samples MA5, MA15, MA17, and MA23 are detected by SEM-EDS. The sediments are dominated SiO_2

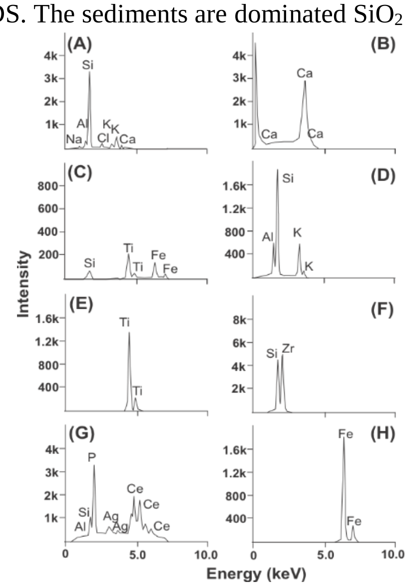

Fig. 2 SEM-EDS compositional data for the Mis Amores beach sediments, Gulf of Mexico. A) quartz and k-feldspar, B) calcite, C) ilmenite, D) k-feldspar, E) calcium sulfate, F) zircon, G) apatite, H) magnetite or hematite, and I) rutile.

content (~ 66-80%), which reveals the abundance of quartz grains (Fig. 2A). The CaO content (~ 3-11%) reveal the presence of calcite and shell fragments in sediments. In sample MA17, Al_2O_3 and K_2O concentrations vary between ~ 3% - 7% and ~ 0.8% - 2.8%, respectively, suggesting the abundance of k- feldspar. Similarly, the TiO_2 and Fe_2O_3 contents vary between 0.7% - 0.24% and 1.11% - 1.84%, respectively. Other mineral phases detected are pyroxene, monzonite, and zircon (Fig. 2 A, F and G). Peaks for sulfur and calcium are detected in samples MA5 and MA17.

GEOCHEMISTRY

The concentrations of major, trace, and rare earth elements are listed in Tables 2, 3, and 4, respectively. The sediments are enriched in SiO_2 content (~ 72.3 wt.% - 85.4 wt.%), which is followed by Al_2O_3 (mean = 5.65 wt.%) and CaO (mean = 5.26 wt.%) contents. The major element concentrations are normalized with respect to the average Upper Continental Crust (UCC) values (Fig. 3; McLennan, 2001).

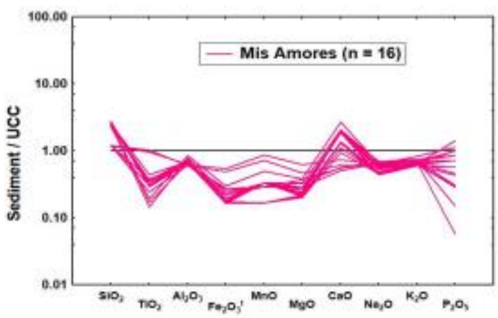

Fig. 3 Diagram showing major element concentrations normalized against average upper continental crust (UCC) values for the Mis Amores beach sediments. Average UCC values are from McLennan (2001).

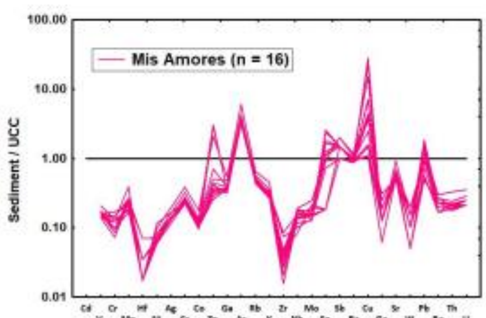

Fig. 4 Upper continental crust (UCC) normalized trace element diagram for the Mis Amores beach sediments. The average UCC values are from McLennan (2001).

The trace element concentrations are also normalized with respect to average UCC values (Fig. 4; McLennan, 2001). Relative to UCC the MA sediments are higher in Zn, As, and Cu contents, and lower in B, Sn, Sb, and B contents, suggesting a lithogenic origin (Armstrong-Altrin et al., 2019). The REE concentrations are normalized with respect to the average Chondrite values (Fig. 5; McLennan, 2001). The Chondrite normalized REE patterns consist slightly negative and positive europium anomalies, and are depleted with respect to UCC (Fig. 5).

ENVIRONMENTAL INDICES

The environmental indices such as EF (Zoller et al., 1974), I_{geo} (Müller, 1969), AEI (Long et al., 1995), and PLI (Tomlinson et al., 1980) were utilized in various studies to assess the pollution level of marine and lake sediments (Ramos-Vázquez et al., 2017; Madadi et al., 2023). In this study, we utilized these environmental indices to infer the variations in elemental concentrations, toxicity, and ecological

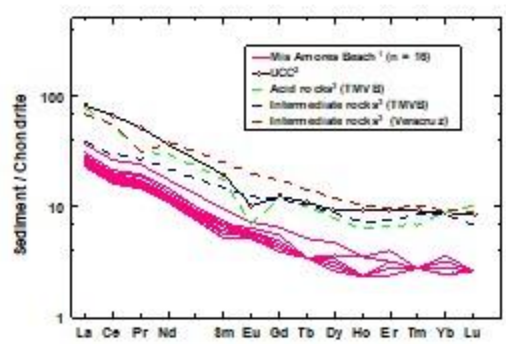

Fig. 5 Chondrite-normalized REE patterns for the Mis Amores beach sediments. Average composition of source rocks: [1] This study, [2] The average UCC values are from McLennan (2001), [3] Verma (2015)

state. According to the obtained values, in Table 5, we assigned different colors to identify the level of contamination, i.e. yellow corresponds to slight enrichment, orange indicates moderate enrichment, and red indicates strong to extreme enrichment.

The EF values vary from 1.21 to 1.57 for Cd (in all samples), 1.27 to 1.43 for Ba (in all samples), and 1.11 to 2.52 for Pb (only in 11 samples). The values with extreme enrichment are in elements Cu (1.49 - 41.47), As (7.19 - 4.86), and Zn (0.37 - 4.28). However, an enrichment is not identified for the elements Cr, Ni, Co and V.

On the other hand, I_{geo} indicated a possible contamination for Zn, Cu, and As with different degrees, i.e. moderate contamination for

Table 2. Major element concentrations (in wt. %) for the Mis Amores beach sediments, Gulf of Mexico

Location	Mis Amores																Statistical parameters		
Sample No.	MA1	MA3	MA5	MA7	MA9	MA11	MA13	MA15	MA17	MA19	MA21	MA23	MA25	MA27	MA29	MA31	n	mean	std
SiO_2	79.13	76.26	72.34	78.26	78.21	78.41	79.38	78.81	80.59	79.7	82.79	83.45	85.42	84.26	80.05	83.37	16	80.03	3.30
TiO_2	0.07	0.06	0.08	0.15	0.15	0.12	0.13	0.13	0.12	0.18	0.13	0.14	0.12	0.13	0.12	0.14	16	0.12	0.03
Al_2O_3	5.35	6.27	6.78	5.86	5.72	5.82	5.49	5.55	5.23	5.51	5.54	5.31	5.45	5.62	5.49	5.43	16	5.65	0.39
$Fe_2O_3^*$	0.61	0.81	1.04	0.67	0.67	0.68	0.63	0.63	0.63	0.75	0.61	0.57	0.58	0.58	0.62	0.61	16	0.67	0.12
MnO	0.02	0.02	0.03	0.02	0.02	0.02	0.02	0.02	0.02	0.02	0.01	0.02	0.01	0.01	0.02	0.02	16	0.02	0.01
MgO	0.31	0.44	0.51	0.38	0.35	0.38	0.35	0.36	0.32	0.36	0.29	0.28	0.27	0.28	0.3	0.29	16	0.34	0.06
CaO	5.92	6.19	7.99	5.69	5.89	5.7	5.7	5.87	5.57	5.77	4.09	3.95	2.82	3.34	5.75	3.94	16	5.26	1.30
Na_2O	1.56	1.98	1.86	1.99	1.74	1.8	1.52	1.62	1.28	1.32	1.4	1.32	1.32	1.35	1.28	1.28	16	1.54	0.26
K_2O	1.78	2.12	2.32	1.98	1.92	1.95	1.83	1.86	1.68	1.75	1.81	1.71	1.76	1.78	1.83	1.74	16	1.86	0.17
P_2O_5	0.1	0.06	0.08	0.06	0.07	0.05	0.07	0.004	0.04	0.05	0.02	0.03	0.05	0.02	0.05	0.04	16	0.05	0.02
LOI	5.14	5.78	6.99	4.93	5.28	5.08	4.9	5.16	4.51	4.59	3.32	3.21	2.19	2.62	4.5	3.14	16	4.46	1.26
Sum	99.99	99.99	100.0	99.99	100.0	100.0	100.0	100	99.99	100	100	99.99	99.99	99.99	100	100	16	100	0.01
Al_2O_3/TiO_2	76.43	104.5	84.75	39.1	38.13	48.50	42.23	42.69	43.58	30.61	42.62	37.9	45.4	43.23	45.75	38.79	16	50.26	20.13
K_2O/Na_2O	1.14	1.07	1.25	0.99	1.10	1.08	1.20	1.15	1.31	1.33	1.29	1.30	1.33	1.32	1.43	1.36	16	1.23	0.12
SiO_2/Al_2O_3	14.79	12.16	10.67	13.3	13.67	13.47	14.46	14.20	15.41	14.46	14.94	15.72	15.67	14.99	14.58	15.35	16	14.24	1.35
K_2O/ Al_2O_3	0.33	0.34	0.34	0.34	0.34	0.34	0.33	0.34	0.32	0.32	0.33	0.32	0.32	0.32	0.33	0.32	16	0.33	0.01
CIW'	83.75	80.24	81.21	80.16	82.21	81.71	84.10	83.23	86.27	85.90	85.17	85.9	85.9	85.62	86.27	86.27	16	83.99	2.25

std = standard deviation; n = total number of samples; *Total Fe expressed as Fe_2O_3; CaO^* = CaO in silicate fraction; CIW = Chemical Index of Weathering ($[Al_2O_3/ (Al_2O_3 + CaO^* + Na_2O)] \times 100$; Harnois, 1988).

Table 3. Trace element concentrations (in ppm) for the Mis Amores beach sediments, Gulf of Mexico

Location	Mis Amores																Statistical parameters		
Sample No.	MA1	MA3	MA5	MA7	MA9	MA11	MA13	MA15	MA17	MA19	MA21	MA23	MA25	MA27	MA29	MA31	n	mean	std
Sc	0.07	0.07	0.15	0.07	0.07	0.07	0.07	0.07	0.07	0.07	0.07	0.07	0.07	0.07	0.07	0.07	16	0.08	0.02
Li	0.50	0.63	0.77	0.58	0.53	0.60	0.53	0.55	0.54	0.55	0.55	0.51	0.56	0.57	0.55	0.54	16	0.56	0.06
Cd	0.00	0.00	0.00	0.00	0.00	0.00	0.00	0.00	0.00	0.00	0.00	0.00	0.00	0.00	0.00	0.00	16	0.00	0.00
V	0.14	0.18	0.21	0.17	0.16	0.16	0.15	0.15	0.15	0.17	0.16	0.14	0.15	0.15	0.15	0.15	16	0.16	0.02
Cr	0.07	0.10	0.13	0.08	0.08	0.14	0.14	0.10	0.10	0.08	0.17	0.12	0.10	0.13	0.12	0.12	16	0.11	0.03
Mn	0.24	0.27	0.39	0.26	0.25	0.26	0.25	0.25	0.23	0.25	0.20	0.21	0.17	0.18	0.24	0.19	16	0.24	0.05
Hf	0.02	0.02	0.02	0.07	0.03	0.02	0.02	0.02	0.07	0.02	0.02	0.02	0.03	0.02	0.02	0.02	16	0.03	0.02
Ni	0.06	0.08	0.10	0.07	0.06	0.06	0.07	0.07	0.07	0.07	0.08	0.08	0.07	0.07	0.08	0.12	16	0.08	0.01
Ag	0.01	0.01	0.01	0.01	0.00	0.00	0.00	0.00	0.00	0.00	0.00	0.00	0.00	0.00	0.00	0.00	16	0.00	0.00
Cs	0.22	0.32	0.38	0.27	0.26	0.27	0.25	0.24	0.24	0.26	0.25	0.22	0.24	0.25	0.26	0.24	16	0.26	0.04
Co	0.09	0.14	0.18	0.12	0.12	0.12	0.11	0.12	0.10	0.11	0.11	0.10	0.11	0.10	0.11	0.11	16	0.11	0.02
Bi	0.00	0.00	0.00	0.00	0.00	0.00	0.00	0.00	0.00	0.00	0.00	0.00	0.00	0.00	0.00	0.00	16	0.00	0.00
Se	0.00	0.00	0.00	0.00	0.00	0.00	0.00	0.00	0.00	0.00	0.00	0.00	0.01	0.00	0.00	0.00	16	0.00	0.00
Zn	2.86	3.03	2.07	0.70	0.38	0.50	0.32	0.36	0.35	0.41	0.44	0.33	0.36	0.26	0.28	0.29	16	0.81	0.94
Ga	0.34	0.34	0.55	0.39	0.35	0.48	0.34	0.37	0.32	0.32	0.39	0.38	0.36	0.36	0.36	0.38	16	0.38	0.06
As	3.67	3.73	6.07	4.27	3.73	4.27	3.87	3.60	3.20	3.73	3.20	4.20	3.33	3.40	4.47	3.27	16	3.88	0.71
Rb	0.43	0.56	0.65	0.53	0.50	0.52	0.48	0.48	0.44	0.46	0.47	0.44	0.47	0.48	0.47	0.45	16	0.49	0.05
Y	0.27	0.36	0.45	0.32	0.30	0.32	0.30	0.29	0.30	0.33	0.29	0.26	0.29	0.27	0.30	0.29	16	0.31	0.04
Zr	0.03	0.03	0.03	0.08	0.05	0.04	0.02	0.02	0.07	0.04	0.03	0.02	0.05	0.04	0.02	0.03	16	0.04	0.02
Nb	0.12	0.18	0.19	0.16	0.17	0.18	0.13	0.14	0.10	0.14	0.16	0.13	0.08	0.17	0.14	0.15	16	0.15	0.03
Mo	0.13	0.17	0.25	0.15	0.14	0.17	0.15	0.14	0.13	0.16	0.15	0.15	0.21	0.15	0.16	0.19	16	0.16	0.03
Sn	1.27	0.91	1.09	2.36	2.55	1.82	1.64	1.09	0.73	0.91	0.18	0.18	0.18	0.18	0.18	0.18	16	0.97	0.80
Sb	1.50	2.00	2.00	1.50	1.50	1.50	1.50	1.50	1.00	1.00	1.50	1.50	1.00	1.50	1.50	1.00	16	1.44	0.31
Ba	0.88	1.08	1.15	1.01	0.99	0.96	0.98	0.94	0.87	0.87	0.95	0.87	0.92	0.94	0.98	0.89	16	0.95	0.08
Cu	27.60	21.88	15.08	7.04	7.00	6.76	4.44	4.24	3.62	4.12	2.45	1.46	1.57	1.04	1.17	1.10	16	6.91	7.87
Ge	0.13	0.13	0.13	0.19	0.13	0.13	0.13	0.13	0.25	0.13	0.13	0.13	0.31	0.06	0.13	0.13	16	0.14	0.06
Ta	0.10	0.10	0.10	0.10	0.10	0.10	0.10	0.10	0.10	0.10	0.10	0.10	0.10	0.10	0.10	0.10	16	0.10	0.00
Sr	0.60	0.69	0.91	0.65	0.62	0.65	0.62	0.63	0.59	0.60	0.54	0.55	0.51	0.53	0.63	0.52	16	0.62	0.10
Pb	1.21	0.99	1.32	1.84	1.76	1.59	1.46	0.95	0.72	0.90	0.91	0.56	0.51	0.50	0.51	0.48	16	1.01	0.47
Th	0.18	0.24	0.33	0.22	0.21	0.22	0.21	0.20	0.19	0.21	0.21	0.19	0.20	0.21	0.20	0.21	16	0.21	0.03
U	0.21	0.29	0.36	0.25	0.25	0.25	0.25	0.25	0.21	0.25	0.25	0.21	0.21	0.21	0.21	0.25	16	0.25	0.04

Table 4. Rare earth element concentrations (in ppm) for the Mis Amores beach sediments, Gulf of Mexico.

Location	Mis Amores																Statistical parameters		
Sample No.	MA1	MA3	MA5	MA7	MA9	MA11	MA13	MA15	MA17	MA19	MA21	MA23	MA25	MA27	MA29	MA31	n	mean	std
La	8.7	11.3	13.5	10.3	9.7	9.7	9.9	9.5	9.2	10.6	9.4	8.4	9.1	9.4	9.5	9.4	16	9.85	1.20
Ce	16.1	20.5	25.3	18.7	17.9	17.6	18.1	17.3	16.9	19.4	17.1	15.5	16.3	17.1	17.4	16.9	16	18.01	2.31
Pr	2.1	2.7	3.3	2.4	2.3	2.3	2.4	2.2	2.2	2.6	2.2	2	2.1	2.2	2.3	2.2	16	2.34	0.31
Nd	8.1	10.4	12.5	9.1	8.9	9	8.9	8.6	8.4	9.7	8.3	7.8	8	8.1	8.6	8.4	16	8.93	1.16
Sm	1.2	1.6	2.2	1.6	1.5	1.3	1.6	1.4	1.5	1.7	1.5	1.2	1.4	1.3	1.6	1.4	16	1.50	0.24
Eu	0.46	0.56	0.63	0.52	0.51	0.51	0.5	0.48	0.47	0.5	0.51	0.46	0.45	0.48	0.51	0.48	16	0.50	0.04
Gd	1.2	1.7	2	1.5	1.4	1.3	1.4	1.3	1.3	1.4	1.3	1.2	1.2	1.2	1.4	1.2	16	1.38	0.21
Tb	0.2	0.2	0.3	0.2	0.2	0.2	0.2	0.2	0.2	0.2	0.2	0.2	0.2	0.2	0.2	0.2	16	0.21	0.03
Dy	1.1	1.4	1.8	1.3	1.2	1.2	1.2	1.3	1.1	1.3	1.2	1	1.1	1.1	1.1	1.1	16	1.22	0.19
Ho	0.2	0.3	0.3	0.2	0.2	0.2	0.2	0.2	0.2	0.2	0.2	0.2	0.2	0.2	0.2	0.2	16	0.21	0.03
Er	0.6	0.8	1	0.7	0.6	0.7	0.6	0.7	0.7	0.8	0.6	0.6	0.6	0.6	0.7	0.7	16	0.69	0.11
Tm	0.1	0.1	0.1	0.1	0.1	0.1	0.1	0.1	0.1	0.1	0.1	0.1	0.1	0.1	0.1	0.1	16	0.10	0.00
Yb	0.6	0.8	0.9	0.7	0.6	0.7	0.6	0.6	0.6	0.7	0.6	0.6	0.6	0.6	0.6	0.6	16	0.65	0.09
Lu	0.1	0.1	0.1	0.1	0.1	0.1	0.1	0.1	0.1	0.1	0.1	0.1	0.1	0.1	0.1	0.1	16	0.10	0.00
LREE	36.2	46.5	56.8	42.1	40.3	39.9	40.9	39	38.2	44	38.5	34.9	36.9	38.1	39.4	38.3	16	40.63	5.18
HREE	4.56	5.96	7.13	5.32	4.91	5.01	4.9	4.98	4.77	5.3	4.81	4.46	4.55	4.58	4.91	4.68	16	5.05	0.67
ΣREE	40.76	52.46	63.93	47.42	45.21	44.91	45.8	43.98	42.97	49.3	43.31	39.36	41.45	42.68	44.31	42.98	16	45.68	5.84
Eu/Eu*	1.160	1.031	0.902	1.011	1.059	1.187	0.999	1.070	1.006	0.963	1.091	1.160	1.036	1.156	1.019	1.105	16	1.06	0.08

n = total number of samples. LREE = Low Rare Earth Elements; HREE = Heavy Rare Earth Elements; TREE = Total Rare Earth Elements

Zn and As. However, Cu indicates contamination in 11 samples with a range between moderate to extreme (average I_{geo} = 2.2). The adverse effect index calculated based on the NOAA reference Tables (with respect to ERL) indicates potentially toxic effects to organisms by Cu in 13 samples (Fig. 6), which is consistent with the I_{geo} results. The PLI reveal that there is a higher pollutant load in a few samples. Based on the environmental indices the trace metals contamination can be ranked in decreasing order: Cu > As > Zn > Cd > Ba.

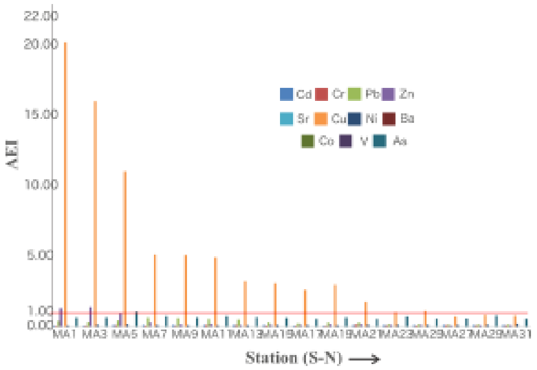

Fig. 6 Adverse Effect Index (AEI) in the Mis Amores beach sediments, Veracruz State, Gulf of Mexico.

DISCUSSION

The grain size variations can provide information on the origin and paleoenvironment. Some authors documented that poorly sorted sediments with positive skewness values are indicators of aeolian transport (Xiong et al., 2010; Jian-Wu et al., 2013). The fine-grained sediments in the MA beach indicate a constant reworking of sediments in the foreshore region due to wind and wave actions. About 16 samples in the MA beach are well-classified, which is probably due to the oscillatory movement of water in the break zone that tends to separate suspended particles (fine-grained) from coarse-grained particles (transported as bed load). On the other hand, the combination of well- classified and very well-classified in samples MA5 and MA11 represent the high influence of wind action. 5 samples are categorized as leptokurtic and 11 as mesokurtic, suggesting long transport of sediments and long distance between the source area and the coast.

The SEM-EDS analysis suggests the abundance of minerals like quartz, calcite, ilmenite, magnetite, titanite, pyroxene, feldspar-K, apatite, and zircon in sediments (Fig. 2A-G). These minerals are detected due to the elevated concentrations of elements like Fe_2O_3, MnO, TiO_2, SiO_2, CaO, (Ce, La, Pr, Nd, Th, and Y), PO_4, and $ZrSiO_4$. Enrichment of some rare earth elements is probably due to the abundance of apatite in sediments.

The SiO_2 content shows negative correlation with elements like Al_2O_3, MgO, K_2O, TiO_2, V, Sr, Rb, REEs, Yb, and Th, which indicates that SiO_2 is controlled by quartz (Ekoa Bessa et al., 2021a). Relative to UCC the MA sediments are enriched in SiO_2 and CaO contents and depleted in remaining elements. The Al_2O_3/TiO_2 ratio values vary from ~ 30.6 to 104.5 and are > 28, which suggests that the sediments

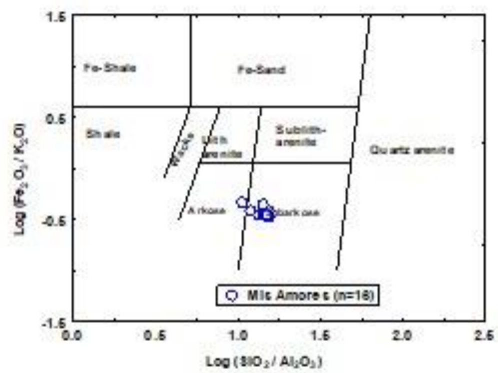

Fig. 7 Geochemical classification of sediments based on log (SiO_2/Al_2O_3) and log(Fe_2O_3/K_2O) ratios (Herron, 1988).

were derived from felsic rocks (Girty et al., 1996). Based on the geochemical classification of Herron (1988), the sediments are classified as subarkose (Fig. 7), suggesting that the sediments are geochemically mature and consistent with the high SiO_2 content (> 75%). A modified weathering index Chemical Index of Weathering (CIW = 80.2 - 86.3) demonstrates a highly weathered sediments derived from a distance source.

The positive correlation of Ba versus K_2O (r = 0.95; n = 16) and Al_2O_3 versus K_2O (0.98; n = 16) reveals their association with k-feldspars (Armstrong-Altrin et al., 2021, 2022). In addition, the positive correlation of Ca against Sr, Rb, and Ba (r = 0.89, r = 0.61, r = 0.59; respectively; n = 16) suggests metal exchange among minerals.

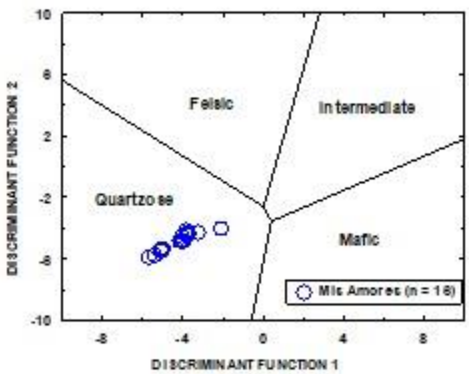

Fig. 8 Provenance discriminant function diagram of Roser and Korsch (1988). The discriminant functions are: Discriminant Function 1 = (− 1.773*TiO_2) + (0.607*Al_2O_3) + (0.760*Fe_2O_3) + (− 1.500*MgO) + (0.616*CaO) + (0.509*Na_2O) + (− 1.224*K_2O) + (−9.090); Discriminant Function 2 = (0.445*TiO_2) + (0.070*Al_2O_3) + (−0.250*Fe_2O_3) + (− 1.142*MgO) + (0.438*CaO) + (1.475*Na_2O) + (1.426*K_2O) + (−6.861).

TiO_2, Fe_2O_3, MnO, and MgO in sediments represent mafic minerals such as magnetite, ilmenite, and rutile (Mohanty et al., 2023). Similarly, enrichment of Ba, Cu, and Zn contents is characteristics of felsic igneous rocks (Tiju et al., 2018). On the provenance discrimination diagram of Roser and Korsch (1986) (Fig. 8), the sediments are classified as felsic igneous and quartzose sedimentary provenances.

Trace element concentrations in clastic sediments are highly useful tool to infer their origin, because incompatible trace elements (Th, U, Pb, Rb, Sr, and Ba) are enriched in sediments derived from felsic igneous rocks, while compatible elements (Ni and Cr) are enriched in mafic igneous rocks (Cullers and Podkovyrov, 2000; Ramos-Vázquez and Armstrong-Altrin,

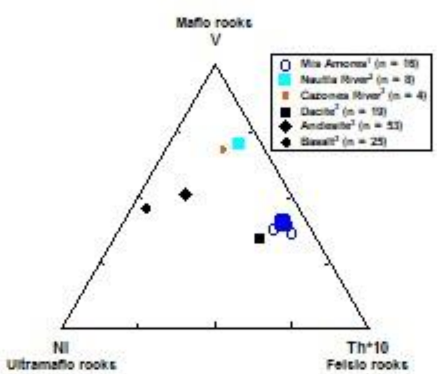

Fig. 9 Ni-Th*10-V ternary diagram for the Mis Amores beach sediments (after Bracciali et al., 2007). Average composition of source rocks: [1] This study, [2] Armstrong-Altrin et al. (2021); [3] Armstrong-Altrin (2009)

2021). The ternary diagram based on trace elements like Ni, Th, and V (Bracciali et al., 2007) reveals a felsic source rock, similar to dacite for the MA beach sediments (Fig. 9). For comparison, on the Ni-Th*10-V ternary diagram the trace element contents of the nearby Nautla and Cazones River samples and source rocks adjacent to the study area are also included (Armstrong-Altrin, 2009) (Fig. 9). The Ni-Th*10-V ternary diagram reveals that the sediments were possibly derived from felsic igneous rocks. This interpretation is consistent with the geology of the Gulf of Mexico coastal area. According to the obtained results, we infer that the source of sediments is dacites and rhyolites in the Trans-

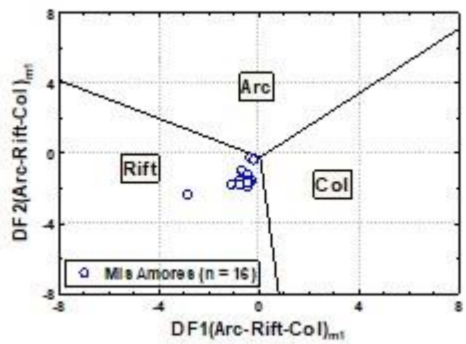

Fig. 10 Tectonic discrimination diagram for the high-silica clastic sediments (SiO_2 = > 63 wt. %; Verma and Armstrong-Altrin, 2013). The subscript m1 in DF1 and DF2 represents the high-silica diagram based on $\log_e$-ratios of major elements. The discriminant function equations are: $DF1_{(Arc\text{-}Rift\text{-}Col)\ m1}$= (−0.263 × In($TiO_2/SiO_2$)$_{adj}$) + (0.604 × In ($Al_2O_3/SiO_2$)$_{adj}$) + (−1.725 × In($Fe_2O_{3t}/SiO_2$)$_{adj}$) + (0.660 × In($MnO/SiO_2$)$_{adj}$) + (2.191 × In($MgO/SiO_2$)$_{adj}$) + (0.144 × In($CaO/SiO_2$)$_{adj}$) + (−1.304 × In($Na_2O/SiO_2$)$_{adj}$) + (0.054 × In($K_2O/SiO_2$)$_{adj}$) + (−0 .33 0 × In ($P_2O_5$ / SiO_2)$_{adj}$) + 1 .588

$DF2_{(Arc\text{-}Rift\text{-}Col)m1}$= (−1.196 × In($TiO_2/SiO_2$)$_{adj}$) + (1.604 × In($Al_2O_3/SiO_2$)$_{adj}$) + (0.303 × In($Fe_2O_{3t}/SiO_2$)$_{adj}$) + (0.436 × In($MnO/SiO_2$)$_{adj}$) + (0.838 × In($MgO/SiO_2$)$_{adj}$) + (−0.407 × In($CaO/SiO_2$)$_{adj}$) + (1.021 × In($Na_2O/SiO_2$)$_{adj}$) + (−1.706 × In($K_2O/SiO_2$)$_{adj}$) + (−0.126 × In($P_2O_5/SiO_2$)$_{adj}$) − 1.068.

Mexican Volcanic Belt and were transported to the beach by the Nautla and Cazones Rivers.

The REE contents of the analyzed sediments are reported in Table 4. The chondrite normalized REE patterns show fractionated LREE with negative europium anomaly (Fig. 5). The europium anomaly is dominated with a weak negative Eu anomaly (Eu/Eu* = ~ 0.9 to 1.19), which signify the domination of felsic source rock with little contribution by andesites. Also, in Figure 5, we compared the REE patterns of Mis Amores sediments with felsic and intermediate rocks from the nearby Trans Mexican Volcanic

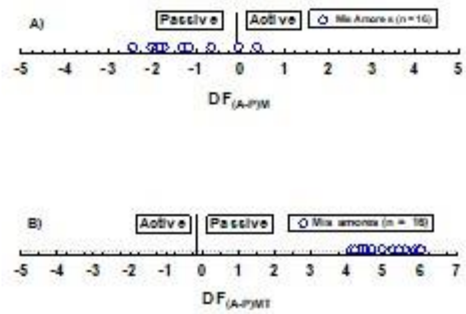

Fig. 11 **A)** Major element (M)-based multidimensional tectonic discriminant function diagram for the discrimination of active (A) and passive (P) margin settings (Verma and Armstrong-Altrin, 2016). The function ($DF_{(A-P)M}$) is to be calculated from the equation $DF_{(AP)M} = (3.0005 * ilr1_{TiM}) + (-2.8243 * ilr2_{AlM}) + (-1.0596 * ilr3_{FeM}) + (-0.7056 * ilr4_{MnM}) + (-0.3044 * ilr5_{MgM}) + (0.6277 * ilr6_{CaM}) + (-1.1838 * ilr7_{NaM}) + (1.5915 * ilr8_{KM}) + (0.1526 * ilr9_{PM}) -5.9948$

B) Major and trace elements (MT) based diagram. The function (DF(AP)MT) is to be calculated from equation: DF(AP) MT = (3.2683 * ilr1TiMT) + (5.3873 * ilr2AlMT) + (1.5546 * ilr3FeMT) + (3.2166 *ilr4MnMT) + (4.7542 * ilr5MgMT) + (2.0390 * ilr6CaMT) + (4.0490 *ilr7NaMT) + (3.1505 * ilr8KMT) + (2.3688 * ilr9PMT) + (2.8354 *ilr10CrMT) + (0.9011 * ilr11NbMT) + (1.9128 * ilr12NiMT) + (2.9094 *ilr13VMT) + (4.1507 * ilr14YMT) + (3.4871 * ilr15ZrMT) - 3.2088. Ilr = isometric log-ratio transformation.

Belt (Verma, 2015). The similarity among REE patterns supports for a felsic provenance. The ΣREE content show a positive correlation with Al_2O_3 ($r = 0.92$; $p < 0.05$; $n = 16$), Fe_2O_3 ($r = 0.98$; $p < 0.05$), MnO ($r = 0.63$; $p < 0.05$), MgO ($r = 0.92$; $p < 0.05$) Th ($r = 0.96$; $p < 0.05$), Ba ($r = 0.83$; $p < 0.05$), Sr ($r = 0.90$; $p < 0.05$), and V ($r = 0.97$; $p < 0.05$), suggesting a similar source for these elements (Madhavaraju et al., 2021).

Furthermore, the major and trace element concentrations in clastic sediments has been widely applied to infer the tectonic setting of an unknown sedimentary basin (Bhatia, 1983; Roser and Korsch, 1986; Verma and Armstrong-Altrin, 2013, 2016). In this study, we utilized the tectonic discrimination diagrams of Verma and Armstrong-Altrin (2013, 2016) (Figs. 10 and 11A and B). On these tectonic discrimination diagrams the Mis Amores sediments plot in the rift and passive margin fields, which suggest a passive margin setting for the Gulf of Mexico sediments. This interpretation is consistent with the tectonic history of the Gulf of Mexico.

The heavy metal concentrations in beach sediments were analyzed in various studies from different parts of the world to infer the level of contamination (Ayala-Pèrez et al., 2021; Ekoa Bessa et al., 2021 b). In this study, we attempt to evaluate the level of trace metal pollution in the MA beach sediments, because we believe that the level of pollutants is increased recently due to the industrialization and uncontrolled urbanization in the coastal regions of the Gulf of Mexico. The trace element patterns normalized with respect to UCC show a notable enrichment of As, Cu, and Zn and these elements are considered as best environmental indicators (Villanueva and Botello, 19988; Velandia-Aquino et al., 2023).

The environmental indices such as EF, I_{geo}, AEI, and PLI reveal a moderate to severe enrichment for As, Zn, and Cu contents, suggesting an anthropogenic source. Sadiq (1992) and Reimann and Caritat (1998) reported that the use of pesticides, herbicides, and fungicides for agricultural activities is responsible for the enrichment of these metals in sediments. Also, an extensive occupation of land along the Tuxpan River basin for agricultural activities (43%) is increased recently. The concentration of metals Cu, As, and Zn in sediments is a potential danger to the local environment (Table 5). The tourist and urban activities in the MA beach area may be responsible for the accumulation of heavy metals in sediments. The concentration of Cu (~ 26 ppm - 690 ppm), also imply its derivation due to industrial, tourism, and recreational activities. In addition, Cu and Zn are related to wastewater discharges that may originate from the nearby Tuxpan City. Zn can be also attributed to activities in the Tuxpan port, because Zn is commonly used in the port infrastructures to prevent the corrosion by seawater (Reimann and Caritat, 1998; Zhou et al., 2024). Similarly, source of As is primarily attributed to agricultural and aqua cultural activities in the coastal area (Gustafsson and Jacks, 1995; Sun et al., 2025). Cu and Zn in sediments may derive from the anti-corrosion coatings, discarded batteries, and printing. However, evidence of contamination attributed to activities associated with oil industry is not observed in this study.

CONCLUSIONS

The Mis Amores beach sediments are very well-sorted and mineralogically mature. The textural parameters reveal a high energy beach environment. The geochemistry data reveal that the sediments were derived from the felsic igneous rocks in the Trans-Mexican Volcanic Belt and transported to the beach by the Tuxpan and Nautla Rivers. The tectonic discrimination diagrams indicated a passive margin setting, which is consistent with the general geology of the southern Gulf of Mexico.

Moderate to severe contamination of Cu, As, and Zn in sediments reflects an intense use of fertilizer and pesticides in the nearby agricultural areas. The enrichment of Zn and As are also associated with the Tuxpan port infrastructure activities. We did not find any contamination in sediments due to oil exploration activity, although is common in the Gulf of Mexico. This study reveals the importance of sediment geochemistry to infer the provenance as well as to understand the level of heavy metal contamination in beach sediments.

Table 5. Comparison of trace metal concentrations in the Mis Amores beach sediments, Gulf of Mexico with environmental indices

Sample	Metal	EF	Igeo	AEI	PLI	Sample	EF	Igeo	AEI	PLI	Sample	EF	Igeo	AEI	PLI	Sample	EF	Igeo	AEI	PLI
	Cd	1.53	-0.56	0.08			1.43	-0.56	0.15			1.57	-0.56	0.08			1.51	-0.56	0.15	
	Cr	0.11	-4.38	0.07			0.12	-4.15	0.09			0.15	-3.96	0.10			0.14	-3.96	0.10	
	Pb	1.82	-0.31	0.44			2.47	0.23	0.64			1.11	-1.05	0.26			0.75	-1.57	0.18	
	Zn	4.30	0.93	1.35			0.53	-1.99	0.18			0.53	-2.11	0.16			0.53	-2.06	0.17	
	Sr	0.91	-1.32	N/A			0.87	-1.27	N/A			0.90	-1.35	N/A			0.75	-1.57	N/A	
MA1	Cu	41.48	4.20	20.29	0.64	**MA9**	9.84	2.22	5.15	0.52	**MA17**	5.56	1.27	2.66	0.44	**MA25**	2.32	0.07	1.16	0.40
	Ni	0.09	-4.67	0.12			0.09	-4.56	0.13			0.11	-4.37	0.15			0.11	-4.37	0.15	
	Ba	1.32	-0.77	N/A			1.39	-0.60	N/A			1.34	-0.78	N/A			1.36	-0.70	N/A	
	Co	0.14	-3.99	N/A			0.17	-3.67	N/A			0.15	-3.91	N/A			0.16	-3.82	N/A	
	V	0.21	-3.42	N/A			0.22	-3.24	N/A			0.23	-3.33	N/A			0.22	-3.33	N/A	
	As	5.51	1.29	0.67			5.25	1.32	0.68			4.92	1.09	0.59			4.92	1.15	0.61	
	Cd	1.31	-0.56	0.08			1.41	-0.56	0.15			1.49	-0.56	0.08			1.46	-0.56	0.15	
	Cr	0.12	-3.96	0.10			0.20	-3.38	0.15			0.12	-4.15	0.09			0.19	-3.50	0.14	
	Pb	1.27	-0.59	0.36			2.19	0.08	0.58			1.31	-0.74	0.33			0.72	-1.58	0.18	
	Zn	3.88	1.01	1.43			0.70	-1.57	0.24			0.60	-1.86	0.20			0.37	-2.55	0.12	
	Sr	0.89	-1.11	N/A			0.90	-1.20	N/A			0.87	-1.33	N/A			0.75	-1.51	N/A	
MA3	Cu	28.06	3.87	16.09	0.71	**MA11**	9.34	2.17	4.97	0.56	**MA19**	6.01	1.46	3.03	0.47	**MA27**	1.49	-0.52	0.77	0.38
	Ni	0.10	-4.20	0.17			0.09	-4.56	0.13			0.10	-4.51	0.14			0.10	-4.37	0.15	
	Ba	1.38	-0.47	N/A			1.32	-0.65	N/A			1.27	-0.79	N/A			1.35	-0.67	N/A	
	Co	0.17	-3.47	N/A			0.17	-3.60	N/A			0.16	-3.75	N/A			0.14	-3.91	N/A	
	V	0.23	-3.08	N/A			0.22	-3.24	N/A			0.25	-3.16	N/A			0.21	-3.33	N/A	
	As	4.79	1.32	0.68			5.89	1.51	0.78			5.45	1.32	0.68			4.86	1.18	0.62	
	Cd	1.21	-0.56	0.15			1.49	-0.56	0.15			1.48	-0.56	0.15			1.49	-0.56	0.15	
	Cr	0.16	-3.50	0.14			0.21	-3.38	0.15			0.24	-3.15	0.17			0.18	-3.64	0.12	
	Pb	1.56	-0.19	0.48			2.14	-0.04	0.53			1.31	-0.73	0.33			0.75	-1.55	0.19	
	Zn	2.46	0.46	0.98			0.46	-2.25	0.15			0.63	-1.79	0.21			0.41	-2.43	0.13	
	Sr	1.08	-0.71	N/A			0.91	-1.27	N/A			0.79	-1.47	N/A			0.93	-1.24	N/A	
MA5	Cu	17.88	3.33	11.09	0.80	**MA13**	6.50	1.57	3.26	0.50	**MA21**	3.56	0.71	1.80	0.47	**MA29**	1.72	-0.36	0.86	0.41
	Ni	0.12	-3.94	0.21			0.10	-4.51	0.14			0.12	-4.20	0.17			0.12	-4.20	0.17	
	Ba	1.37	-0.38	N/A			1.43	-0.62	N/A			1.38	-0.66	N/A			1.43	-0.62	N/A	
	Co	0.21	-3.09	N/A			0.16	-3.75	N/A			0.15	-3.82	N/A			0.16	-3.82	N/A	
	V	0.24	-2.87	N/A			0.22	-3.33	N/A			0.23	-3.24	N/A			0.22	-3.33	N/A	
	As	7.19	2.02	1.11			5.66	1.37	0.71			4.64	1.09	0.59			6.54	1.57	0.82	
	Cd	1.40	-0.56	0.15			1.48	-0.56	0.15			1.55	-0.56	0.15			1.51	-0.56	0.15	
	Cr	0.12	-4.15	0.09			0.14	-3.96	0.10			0.18	-3.64	0.12			0.18	-3.64	0.12	
	Pb	2.52	0.29	0.67			1.38	-0.65	0.35			0.86	-1.41	0.21			0.71	-1.64	0.18	
	Zn	0.97	-1.09	0.33			0.53	-2.05	0.17			0.51	-2.17	0.16			0.43	-2.38	0.14	
	Sr	0.89	-1.22	N/A			0.91	-1.25	N/A			0.83	-1.46	N/A			0.77	-1.52	N/A	
MA7	Cu	9.66	2.23	5.18	0.57	**MA15**	6.14	1.50	3.12	0.47	**MA23**	2.20	-0.04	1.07	0.40	**MA31**	1.63	-0.44	0.81	0.39
	Ni	0.10	-4.41	0.15			0.10	-4.41	0.15			0.12	-4.24	0.17			0.17	-3.69	0.24	
	Ba	1.38	-0.58	N/A			1.36	-0.67	N/A			1.31	-0.79	N/A			1.32	-0.75	N/A	
	Co	0.17	-3.60	N/A			0.17	-3.67	N/A			0.15	-3.91	N/A			0.16	-3.82	N/A	
	V	0.23	-3.16	N/A			0.22	-3.33	N/A			0.21	-3.42	N/A			0.22	-3.33	N/A	
	As	5.85	1.51	0.78			5.22	1.26	0.66			6.36	1.49	0.77			4.84	1.12	0.60	

Yellow = slight enrichment; orange = moderate enrichment; red = strong to extreme enrichment

CREDIT AUTHORSHIP CONTRIBUTION STATEMENT

Mayla A. Ramos-Vázquez: Writing – review and editing, Investigation, Logistic fieldwork, Data curation, Methodology, Validation. **John S. Armstrong-Altrin**: Writing - review and editing, Formal analysis, Resources, Funding acquisition. **Gloria D. Fernández-Guevara:** logistic fieldwork, data curation, methodology, formal analysis, analysis. **Jayagopal Madhavaraju:** Methodology, Formal Analysis, Editing. **Sanjeet K. Verma:** Methodology, Formal Analysis, Review and Editing. **Rathinam Arthur James:** Data curation, Methodology, Formal analysis. All authors contributed equally in writing.

DECLARATION OF COMPETING INTEREST

The authors declare that they have no known competing financial interests or personal relationship that could have appeared to influence the work reported in this paper.

ACKNOWLEDGEMENT

Ramos-Vázquez extends her gratitude to CONAHCyT for the postdoctoral fellowship (CVU: 595593). Armstrong-Altrin acknowledge the financial support extended by the CONAHCyT (no: A1-S-21287) and PAPIIT (IN-104824) projects. We are grateful to Carlos Linares López, Laura E. Gómez Lizárraga, and Arturo Ronquillo Arvizu for their laboratory assistance during the course of this study. This work was initiated during the sabbatical period of John S. Armstrong-Altrin (2023), which was approved by DGAPA (PASPA), UNAM.

REFERENCES

Aquino-Gaspar, H.M., Díaz-Ovalle, Ch.O., López-Molina, A., Conde-Mejía, C. and Valenzuela-Gómez, L.M. (2021). Incident analysis of the "Pajaritos" petrochemical complex. Journal of Loss Prevention in the Process Industries, v. 70, no. 104404.

Armstrong-Altrin, J.S. (2009). Provenance of sands from Cazones, Acapulco, and Bahía Kino beaches, Mexico. Revista Mexicana de Ciencias Geológicas, v. 26(3), pp. 764-782.

Armstrong-Altrin, J.S. (2020). Detrital zircon U-Pb geochronology and geochemistry of the Riachuelos and Palma Sola beach sediments, Veracruz State, Gulf of Mexico: a new insight on palaeoenvironment. Journal of Palaeogeography, v. 9 (4), pp. 28.

Armstrong-Altrin, J.S., Lee, Y.I., Kasper-Zubillaga, J.J., Carranza-Edwards, A., Garcia, D., Eby, N., Balaram, V. and Cruz-Ortiz, N.L. (2012). Geochemistry of beach sands along the Western Gulf of Mexico, Mexico: Implication for provenance. Chemie der Erde Geochemistry, v. 72, pp. 345-362.

Armstrong-Altrin, J.S., Madhavaraju, J., Vega-Bautista, F., Ramos-Vazquez, M.A., PérezAlvarado, B.Y., Kasper-Zubillaga, J.J. and Ekoa Bessa, A.Z. (2021). Mineralogy and geochemistry of Tecolutla and Coatzacoalcos beach sediments, SW Gulf of Mexico. Applied Geochemistry, v. 134, no.105103.

Armstrong-Altrin, J.S., Ramos-Vázquez, M.A., Hermenegildo-Ruiz, N.Y. and Madhavaraju, J. (2021). Microtexture and U-Pb geochronology of detrital zircon grains in the Chachalacas beach, Veracruz State, Gulf of Mexico. Geological Journal, v. 56(5), pp. 2418-2438.

Armstrong-Altrin, J.S., Ramos-Vázquez, M.A., Madhavaraju, J., Marca-Castillo, M.E., Machain-Castillo, M.L. and Márquez-Garcia, A.Z. (2022). Geochemistry of marine sediments adjacent to the Los Tuxtlas Volcanic Complex, Gulf of Mexico: Constraints on weathering and provenance. Applied Geochemistry, v. 141, no. 105321.

Armstrong-Altrin, J.S., Ramos-Vázquez, M.A., Zavala-Léon, A.C. and Montiel-García, P.C. (2018). Provenance discrimination between Atasta and Alvarado beach sands, western Gulf of Mexico, Mexico: constraints from detrital zircon chemistry and U-Pb geochronology. Geological Journal, v. 53(6), pp. 2824-2848.

Ayala-Pérez, M.P., Armstrong-Altrin, J.S. and Machain-Castillo, M.L. (2021). Heavy metal contamination and provenance of sediments recovered at the Grijalva River delta, southern Gulf of Mexico. Journal of Earth System Science, v. 130, article no. 88

Bela, V.A., Bessa, A.Z.E., Armstrong-Altrin, J.S., Kamani, F.A., Nya, E.D.B. and Ngueutchoua, G. (2023). Provenance of clastic sediments: A case study from Cameroon, Central Africa. Solid Earth Sciences, v. 8(2), pp. 105-122.

Bhatia, M.R. (1983). Plate tectonics and geochemical composition of sandstones. Journal of Geology, v. 91, pp. 611-627.

Botello, A.V., Ponce-Vélez, G., Armstrong-Altrin, J.S., Fragoso, S.V. and Velandia-Aquino, L.B. (2023). Concentration of polycyclic aromatic hydrocarbons (PAHs) in sediments from the Tampamachoco lagoon, Tuxpan River mouth, Gulf of Mexico. Arabian Journal of Geosciences, v. 16, no. 556.

Bracciali, L., Marroni, M., Pandolfi, L. and Rocchi, S. (2007). Geochemistry and petrography of Western Tethys Cretaceous sedimentary covers (Corsica and Northern Apennines): from source areas to configuration of margins. In: Arribas, J., Critelli, S., Johnsson, M. J. (Eds.), Sedimentary Provenance and Petrogenesis: Perspectives from Petrography and Geochemistry Geological Society of America Special Paper, vol. 420, pp. 73-93.

Cai, P., Cai, G., Yang, J., Li, X., Lin, J., Li, S. and Zhao, L. (2023). Distribution, risk assessment, and quantitative source apportionment of heavy metals in surface sediments from the shelf of the northern South China Sea. Marine Pollution Bulletin, v. 187, n. 114589.

Cullers, R. and Podkovyrov, V. (2000). Geochemistry of the Mesoproterozoic Lakhanda shales in southeastern Yakutia, Russia: implications for mineralogical and provenance control, and recycling. Precambrian Research, v. 104, pp. 77-93.

Davis, R.A. and Fitzgerald, D.M. (2020). Beaches and Coasts. Wiley. 2nd edition.

Ekoa Bessa, A.Z., Nguetchoua, G., Janpou, A. K., El-Amier, Y.A., Nguetnga, O.N.N.M., Kayou, U.R., Bisse, S. B., Mapuna, E.C.N. and Armstrong-Altrin, J.S. (2021a). Heavy metal contamination and its ecological risks in the beach sediments along the Atlantic Ocean (Limbe coastal fringes, Cameron). Earth Systems and Environment, v. 5, pp. 433-444.

Ekoa Bessa, A. Z., Paul-Désiré, N., Fuh, G.C., Armstrong-Altrin, J.S. and Betsi, T.B. (2021b). Mineralogy and geochemistry of the Ossa lake Complex sediments, Southern Cameroon:

Implications for paleoweathering and provenance. Arabian Journal of Geosciences, v. 14, Article no. 322.

Folk, R.L. and Ward, W.C. (1957). Brazos River Bar: A study in the significance of grain size parameters. Journal of Sedimentary Petrology, v. 27, pp. 3-26.

Girty, G., Ridge, D., Knaack, C., Johnson, D. and Al-Riyami, R. (1996). Provenance and depositional setting of Paleozoic Chert and Argillite, Sierra Nevara, California. Journal of Sedimentary Research, v. 66, pp. 107-118.

Gülşen-Rothmund, H.I., Arslan, Ş., Kurtuluş, B., Tunca, E., Avşar, U. and Avşar, Ö. (2023). Assessment of trace metal pollution in the coastal sediments of Fethiye-Göcek Bay (SW Turkey) and evaluation of pollution sources. Marine Pollution Bulletin, v. 186, no. 114387.

Gustafsson, J.P. and Jacks, G. (1995). Arsenic geochemistry in forested soil profiles as revealed by solid-phase studies. Applied Geochemistry, v. 10, pp. 307-315.

Herron, M. (1988). Geochemical classification of terrigenous sands and shales from core or log data. Journal of Sedimentary Petrology, v. 58, pp. 820-829.

Instituto Nacional de Estadística y Geografía (2016). Estudio de información integrada de la Cuenca del Río Tuxpan. INEGI, 99.

Instituto Nacional de Ecología y Cambio Climático (2018). Plan de Acción para el Manejo Integral de Cuencas Hídricas (PAMIC): Cuenca del Río Tuxpan. INECC, 109.

Jarvis, K.E. (1988). Inductively coupled plasma mass spectrometry: A new technique for the rapid or ultra level determination of the rare-earth elements in geological materials. Chemical Geology, v. 68, pp. 31-39.

Jian-Wu, L., Wei, Y., Gan-Lin, Z., Li-Dong, Z., Yong-Jian, J. and Zi-Tong, G. (2013). Grain Size Evidence of Multiple Origins of Red Clays in the Jinhua-Quzhou Basin, South China. Pedosphere, v. 23(5), pp. 686-695.

Jiang, Ch., Li, Y., Li, Ch., Zheng, L. and Zheng, L. (2022). Distribution, source and behavior of rare earth elements in surface water and sediments in a subtropical freshwater lake influenced by human activities. Environmental Pollution, v. 313, no.

Long, E.R., Macdonald, D.D., Smith, S.L. and Calder, F.D. (1995). Incidence of adverse biological effects within ranges of chemical concentrations in marine and estuarine sediments. Environmental Management, v. 19, pp. 81-97.

Madadi, R., Mejjad, N. and De-la-Torre, G.E. (2023). Geochemical speciation, ecological risk, and source identification of heavy metal(loid)s in sediments and waters from Musa Estuary, Persian Gulf. Marine Pollution Bulletin, v. 190, no. 114836.

Madhavaraju, J., Armstrong-Altrin, J.S., Pillai, R.B. and Pi-Puig, T. (2021). Geochemistry of sands from the Huatabampo and Altata beaches. Gulf of California, Mexico. Geological Journal, v. 56, pp. 2398-2417.

Martínez, M.L., Intralawan, A., Vázquez, G., Pérez-Maqueo, O., Sutton, P. and Landgrave, R. (2007). The coasts of our world: ecological, economic and social importance. Ecological Economics, v. 63(2-3), pp. 254-272.

McLennan, S.M. (2001). Relationship between the trace element composition of sedimentary rocks and upper continental crust. Geochemistry Geophysics Geosystems, v. 2(4).

Mohanty, S., Adikaram, M., Sengupta, D., Madhubashini, N., Wijesiri, Ch., Adak, S., Bera, B. (2023). Geochemical, mineralogical and textural nature of beach placers, north-east Sri Lanka: Implications for provenance and potential resource. International Journal of Sediment Research, v. 38(2), pp. 279-293.

Müller, G. (1969). Index of geoaccumulation in sediments of the Rhine River. Geological Journal, v. 2, pp. 109-118.

Nagarajan, R., Anandkumar, A., Hussain, S.M., Jonathan, M.P., Ramkumar, Mu, Eswaramoorthi, S., Saptoro, A. and Chua, H.B. (2019). Geochemical characterization of beach sediments of the NW Borneo, SE Asia: implications on provenance, weathering intensity and assessment of coastal environmental status. In: Ramkumar, Mu, Arthur James, R., Menier, D., Kumaraswamy, K. (Eds.), Coastal Zone Management: Global Perspectives, Regional Processes, Local Issues. Elsevier, pp. 279-330.

Nikunj, K., Shivam, M., Chandrakant, G. and Laxman, M. (2023). Texture and major element geochemistry of channel sediments in the Orsang and Hiren River Basins, Gujarat, India: Implications for provenance and weathering. Journal of the Indian Association of Sedimentologists, v. 40 (II), pp. 57-67.

Paul, A.Q., Dar, S.A., Singh, B.P., Kumar, H. and Ahmad, M. (2023). Geochemistry of recent sediments of the Kurheri basin, Son River, Madhya Pradesh, Central India: implications for source area weathering, sediment provenance, maturity, and sorting. International Journal of Earth Sciences (Geol Rundsch), v. 112, pp. 1803-1821.

Reimann, C. and Caritat, P. (1998). Chemical elements in the environment: fact sheets for the geochemist and environmental scientist. Berlin: Springer.

Ramos-Vázquez, M.A. and Armstrong-Altrin, J.S. (2019). Sediment chemistry and detrital zircon record in the Bosque and Paseo del Mar coastal areas from the southwestern Gulf of Mexico. Marine and Petroleum Geology, v. 110, pp. 650-675.

Ramos-Vázquez, M.A. and Armstrong-Altrin, J.S. (2021). Provenance of sediments from Barra del Tordo and Tesoro beaches, Tamaulipas State, northwestern Gulf of Mexico. Journal of Palaeogeography, v. 10(20), pp. 1-17.

Ramos-Vázquez, M.A., Armstrong-Altrin, J.S., Machain-Castillo, M.L. and Gío-Argáez, F.R. (2018). Foraminiferal assemblages, ^{14}C ages, and compositional variations in two sediment cores in the western Gulf of Mexico. Journal of South American Earth Sciences, v. 88, pp. 480-496.

Ramos-Vázquez, M.A., Armstrong-Altrin, J.S., Rosales-Hoz, L., Machain-Castillo, M.L. and Carranza-Edwards, A. (2017). Geochemistry of deep-sea sediments in two cores retrieved at the mouth of the Coatzacoalcos river delta, Western Gulf of Mexico, Mexico. Arabian Journal of Geosciences, v. 10, pp. 148.

Ramos-Vázquez, M.A., Armstrong-Altrin, J.S., Madhavaraju, J., Gracia, A., Salas-de-León, D.A. (2022). Mineralogy and geochemistry of marine sediments in the Northeastern Gulf of Mexico. In: Armstrong-Altrin JA, Pandarinath K, Verma S. (Eds.), Geochemical Treasures and Petrogenetic Processes. pp. 153-183.

Resmi, M.R. and Achyuthan, H. (2018). Lower Palar River Sediments, Southern Peninsular, India: Geochemistry, Source-Area Weathering, Provenance and Tectonic Setting. Journal of the Geological Society of India, v. 92, pp. 83-91.

Roser, B. and Korsch (1986). Determination of tectonic setting of sandstone-mudstone suites using SiO_2 content and K_2O/Na_2O ratio. Journal of Geology, v. 94, pp. 635-650.

Roser, B.P. and Korsch, R.J. (1988). Provenance signatures of sandstone-mudstone suites determined using discrimination function analysis of major element data. Chemical Geology, v. 67, pp. 119-39.

Sadiq, M. (1992). Toxic metal chemistry in marine environments. New York: Marcel Dekker.

Sun, Y., Zhang, X., Peng, H., Zhou, W., Jiang, A., Zhou, F., Wang, H. and Zhan, W. (2025). Development of a coupled model to simulate and assess arsenic contamination and impact factors in the Jinsha River Basin, China. Journal of Environmental Science, v. 147, pp. 50-61.

Tapia-Fernandez, H.J., Armstrong-Altrin, J.S. and Selvaraj, K. (2017). Geochemistry and U-Pb geochronology of detrital zircons in the Brujas beach sands, Campeche, Southwestern Gulf of Mexico, Mexico. Journal South American Earth Sciences, v. 76, pp. 346-361.

Tawfik, H.A., Salah, M.K., Maejima, W., Armstrong-Altrin, J.S., Abdel-Hameed, A-M.T. and Ghandour M.M.E. (2018). Petrography and geochemistry of the Lower Miocene Moghra sandstones, Qattara Depression, north Western Desert, Egypt. Geological Journal, v. 53, pp. 1938-1953.

Taylor, S.R. and McLennan, S.M. (1985). The Continental Crust: Its Composition and Evolution. lackwell Publishing, Oxford, UK, p. 312

Tiju, I.V., Prakash, T.N., Nagendra, R. and Nagarajan, R. (2018). Sediment geochemistry of coastal environments, southern Kerala, India: implication for provenance. Arabian Journal of Geosciences, v. 11(61).

Tomlinson, D.L., Wilson, J.G., Harris, C.R. and Jeffrey, D.W. (1980). Problems in the assessment of heavy metal level in estuaries and the formation of pollution index. Helgoland Marine Research, v. 33, pp. 566-575.

Velandia-Aquino, L.B., Botello, A.V., Ponce-Vélez, G., Namihira-Santillán, P.E., Villanueva-Fragoso, S. (2023). Vertical Distribution of Potentially Toxic Metals and PAHs in the Alvarado Lagoon, Veracruz in the Southern Gulf of Mexico. Estuaries and Coasts. https://doi.org/10.1007/s12237-023-01307-6.

Verma, S.P. (2015). Origin, evolution, and tectonic setting of the eastern part of the Mexican Volcanic Belt and comparison with the central American volcanic arc from conventional multielement normalized and new multidimensional discrimination diagrams and discordancy and significance tests. Turkish Journal of Earth Sciences, v. 24, pp. 111-164.

Verma, S.P. and Armstrong-Altrin, J.S. (2013). New multi-dimensional diagrams for tectonic discrimination of siliciclastic sediments and their application to Precambrian basins. Chemical Geology, 355, pp. 117-133.

Verma, S.P. and Armstrong-Altrin, J.S. (2016). Geochemical discrimination of siliciclastic sediments from active and passive margin settings. Sedimentary Geology, v. 332, pp. 1-12.

Villanueva, F.S. and Botello, A.V. (1998). Metal Pollution in Coastal Areas of Mexico. In: Ware, G.W. (eds.) Reviews of Environmental Contamination and Toxicology. Reviews of

Environmental Contamination and Toxicology, vol 157. Springer, New York, NY.

Wang, Z., Wang, J., Fu, X., Zhan, W., Armstrong-Altrin. J.S., Yu, F., Feng, X., Song, C. and Zeng, S. (2018). Geochemistry of the Upper Triassic black mudstones in the Qiangtang Basin, Tibet: Implications for paleoenvironment, provenance, and tectonic setting. Journal of Asian Earth Sciences, v. 160, pp. 118-135.

Xiong, S., Ding, Z., Zhu, Y., Zhou, R. and Lu, H. (2010). A ~ 6 Ma chemical weathering history, the grain size dependence of chemical weathering intensity, and its implications for provenance change of the Chinese loess–red clay deposit. Quaternary Science Reviews, v. 29(15-16), pp. 1911-1922.

Yang, L., Ma, X., Luan, Z. and Yan, J. (2021). The spatial-temporal evolution of heavy metal accumulation in the offshore sediments along the Shandong Peninsula over the last 100 years: Anthropogenic and natural impacts. Environmental Pollution, v. 15(289), no. 117894.

Zavala, J. and Morey, O'Brien (2003). Seasonal circulation on the western shelf of the Gulf of Mexico using a high-resolution numerical model. Journal of Geophysical Research, v. 108(C12), no. 3389.

Zavala, J., Romero, R., Mateos, A. and Morey, S. (2014). The response of the Gulf of Mexico to wind and heat flux forcing: What has been learned in recent years? Atmósfera, v. 27(3), pp. 317-334.

Zhou, Y., Du, S., Liu, Y., Yang, T., Liu, Y., Li, Y. and Zhang, L. (2024). Source identification and risk assessment of trace metals in surface sediment of China Sea by combining APCA-MLR receptor model and lead isotope analysis. Journal of Hazardous Materials, v. 465, no. 133310.

Zoller, W.H., Gladney, E.S. and Duce, R.A. (1974). Atmospheric concentrations and sources of trace metals at the South Pole. Science, v. 183, pp. 198-200.